Three-Dimensional Structures in Laminar Natural Convection in a Cubic Enclosure

W. J. Hiller
S. Koch
T. A. Kowalewski
Max-Planck-Institut für Strömungsforschung, Göttingen, Federal Republic of Germany

The thermal convection in a cubic cavity, with two opposite vertical walls kept at prescribed temperatures, is investigated experimentally. The Rayleigh numbers ranged from 10^4 to 2×10^7 and the Prandtl numbers from 5.8 to 6×10^3. The velocity and vorticity fields are shown. The temperature fields were visualized with the help of liquid crystals suspended as small tracer particles in the medium. It is observed that convection in the cavity is strongly three-dimensional. The streamlines spiral from the foci on the walls toward the foci in the vertical midplane and vice versa. The disappearance of one of the vortices midway between the center and the front or back wall is observed for $Ra > 6 \times 10^4$. The topological structures are discussed. The experimental observations are compared with numerical calculations found in the literature.

Keywords: *natural convection, rectangular enclosures*

INTRODUCTION

It is obvious that convective flows, as well as fluid motion in general, are three-dimensional. However, the limitations of mathematical analyses and experimental techniques have led to a very common trend of approximating convective flows by two-dimensional models. The experimental simulation and mathematical modeling of two-dimensional convective flows have created many flow structures that do not appear to be comparable with real, three-dimensional flows. Several numerical methods for solving the three-dimensional Navier–Stokes equation have been recently developed. Each of these methods enables one, within the limitations of the approximations involved, to produce complete solutions describing three-dimensional flow fields. However, very small changes in the initial and boundary conditions and the existing singularities often give rise to a great number of possibly bifurcating solutions.

The task of choosing the appropriate bifurcations can be eased by the availability of a topological description of the flow field. To obtain such a description, accurate observations of the flow field are needed that include visualization of the different elementary flow patterns to identify the field's critical points and the streamlines in their vicinity. The aim of the present experiments is to find the flow structures for the case of three-dimensional thermal convective flow in a cubic cavity with two opposite vertical walls kept at different temperatures. In addition to its theoretical interest, this type of convective flow has numerous possible applications, among which probably the most widely known is that of double glazing. Other applications can be found in nuclear reactors, energy storage containers, ventilation of room and crystal growth in liquids. However, despite all the recent research activities, a central problem remains unsolved. The flow pattern cannot be predicted a priori from the given geometry and boundary conditions. Thus, in practical applications fluid mechanics usually offers only a simplified, global description of the heat exchange process. It seems that our visualization technique, based on the application of unencapsulated liquid crystals as tracer particles, can be very helpful in analyzing the complicated flow structures that exist in real flows.

NATURAL CONVECTION IN AN ENCLOSED CAVITY

Natural convection in a rectangular enclosure with vertical side walls of different temperatures was first investigated by Batchelor [1]. From his analytical studies, he concluded that various flow regimes exist depending on two dimensionless parameters, namely, the Rayleigh number

$$\mathrm{Ra} = \frac{g\beta d^3 (T_h - T_c)}{\alpha \nu} \tag{1}$$

and the Prandtl number,

$$\mathrm{Pr} = \nu/\alpha \tag{2}$$

and the geometry of the cavity. In the above definitions, g denotes gravitational acceleration, d is the cavity dimension, T_h and T_c are the vertical wall temperatures, α is the thermal diffusivity, β is the coefficient of thermal expansion, and ν is the kinematic viscosity.

Heat is transported from the hot to the cold wall essentially by conduction when the Rayleigh number is small or moderately large. For large Rayleigh numbers, a core of uniform temperature and vorticity was assumed to exist in the central region of the cavity, surrounded by a continuous boundary layer. The Prandtl number is a material property of the fluid, and for liquids with $\mathrm{Pr} > 10$ its influence on the convection flow is relatively small [2, 3].

Several attempts to obtain numerical solutions of the relevant equations followed Batchelor's analysis. Usually, it is assumed that the flow is two-dimensional and that the temperature difference $\Delta T = T_h - T_c$ is sufficiently small

Address correspondence to W. J. Hiller, Max-Planck-Institut für Strömunsforschung, 3400 Göttingen, FRG.

Experimental Thermal and Fluid Science 1989; 2:34–44

0894-1777/89/$3.50

that the Boussinesq approximation may be applied. This means that density and viscosity variations are neglected in the inertial terms of the equation of motion and only density variations in the buoyancy term are considered. From these numerical analyses [4–6], it appears that at relatively small Rayleigh numbers ($Ra < 10^3$) the heat transfer is due mainly to the heat conduction of the medium and the corresponding isotherms are parallel to the heated walls. The temperature gradient is positive everywhere in this case, giving rise to the generation of positive vorticity. The streamlines are those of a single vortex with its center at the center of the cavity. As the Rayleigh number increases ($Ra > 10^3$), the heat transfer due to convection begins to play a significant role, generating a vertical temperature gradient in the center of the cavity. The horizontal gradient of temperature diminishes in the center and, for further increases in the Rayleigh number ($Ra > 6 \times 10^4$), becomes locally negative, promoting the generation of negative vorticity in the core. This causes elongation of the central streamlines in the horizontal direction and the development of a second vortex in the core. A three-dimensional numerical study of this problem was presented by Mallinson and de Vahl Davis [3]. Their calculation confirms the existence of the secondary roll as an effect of dominating convection. According to their calculations, the flow field in the cavity appears strongly three-dimensional, with spiraling streamlines transporting fluid from the core to side walls and back.

Most of the experimental investigations of natural convection in an enclosure are limited to cavities with a high aspect ratio. It is then assumed that the flow field is two-dimensional (see, eg [Refs. 7 and 8]). As a result, not much is known experimentally about the form or significance of the three-dimensional effects that occur in a real flow.

EXPERIMENT

Experimental Facility

The thermal convective flow was generated in a 38 × 38 × 38 mm cubic cavity. Figure 1 shows the cavity and the coordinate system used. The z direction is vertically upwards. Two opposite lateral walls of the box ($y = 0$ and $y = d$) were made of copper and kept at a prescribed temperature by two Peltier elements. The four other walls, made from 8 mm Perspex, were considered to be thermal insulators. The great thermal capacity and thermal conductivity of the copper walls allowed us to maintain constant and uniform temperatures of the heated and cooled walls. These temperatures were continuously measured by means of thermocouples and recorded by a Philips multichannel recorder. The observed temperature fluctuations were less than 0.1°C. The temperature difference between the heated and cooled walls was varied in the range between 2.5°C and 18°C. The mean value of the temperature at the walls was about 29°C. The cavity was filled with glycerol and gylcerol–water solutions as working fluids. These conditions resulted in a Rayleigh number range of 10^4 to 2×10^7 and a Prandtl number range of 6×10^3 to 5.8.

Flow Visualization

Flow structures were visualized using photographic records of the motion of tracer particles illuminated by a sheet of white light. Liquid crystals were used as tracer particles. This visualization method, previously described in [Ref. 9], permits

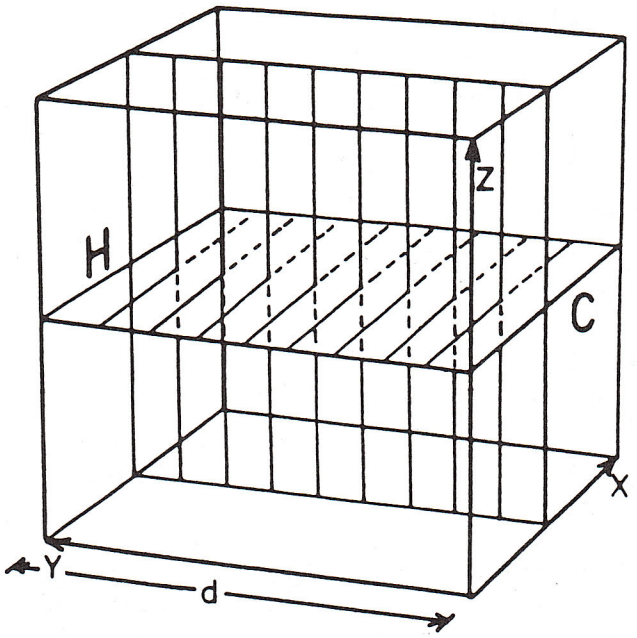

Figure 1. Scheme of the cavity. H, C are the heated and cooled walls, respectively. Visualization of the flow in the horizontal (XY) planes and vertical (YZ) planes.

simultaneous and detailed quantitative measurements of the temperature and velocity field of the flow. Due to the angular selectivity of the light refracted by liquid crystals, these tracers, almost invisible in diffused light, give bright colorful traces when directly illuminated. The liquid crystals respond to a change of temperature by altering the wavelength of the refracted light. Thus, when liquid crystals are illuminated by a parallel beam of white light, their color will change continuously from red to blue within a typical temperature range of a few kelvin. For visualization purposes, liquid crystals are commercially available in two forms—as pure substance or encapsulated in small plastic balls, which are usually suspended in water. They are more stable and chemically resistant in the second form, but we found that only unencapsulated liquid crystals give bright and pure enough colors of refracted light to be suitable for qualitative measurements of temperature. The liquid crystals used here are chiral nematics type TM 107 (BDH Chemicals Ltd.) The red color starting temperature given by the manufacturer is 27°C, and the color play temperature range covers 6°C. This substance was dissolved in ether and dispersed into small droplets. While the droplets were falling within a tube onto a surface of glycerol, the ether evaporated. In this way we produced almost monodisperse suspensions of liquid crystal particles in glycerol. The typical size of the particles was 50 μm, and their concentration in the working fluid was kept below 0.01% by weight. The colors of liquid crystals depend not only on the temperature but also on the angle of refraction and thus on the angle of observation. Therefore, the color play function $\lambda(T)$ of the liquid crystal suspension used has to be separately calibrated under the same observation conditions as in the cavity tested. Figure 2 shows the calibration curve for a suspension of liquid crystals in pure glycerol observed perpendicularly to the direction of the illumination. The calibration curve shows that in our case the full color change takes place over a range of about 2°C. In practice, the angle of observation always has a finite width that

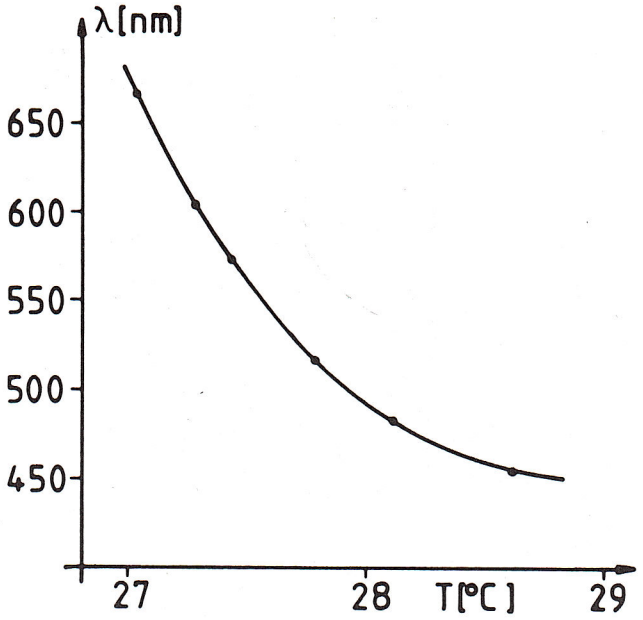

Figure 2. Calibration curve of the wavelength λ of the reflected light as a function of temperature of the liquid crystals suspended in glycerol. Observation at 90° with respect to the direction of the incident light.

generally depends on the distance between the object and the point of observation. This is one of the factors limiting the accuracy of the temperature measurements. We can estimate these errors with the help of previous measurements [9], where we checked the influence of observation angle on temperature measured. In the present measurements, the width of the observation angle was about 3°, from which it follows that the uncertainty in the measured temperature is below 0.1°C.

In the present experiments, we are interested only in the shape of the isotherms and not in their absolute temperature values. For such measurements, one needs another procedure, for instance, a light source of discrete color spectrum. The isotherms presented in the figures are lines of constant color, which are numbered from 1 to 4. They can be interpreted approximately in the following way:

1 Blue (450 nm) ~ 28.8°C 2 Green (540 nm) ~ 27.8°C
3 Yellow (580 nm) ~ 27.4°C 4 Red (660 nm) ~ 27.0°C

Observation Technique

The illumination of the flow was performed by white light of a specially constructed high power (1 kW s) xenon arc flash lamp. Using a cylindrical lens and a slit, a plane sheet of light with a width adjustable in the range of 2–10 mm is obtained. The flash was triggered by a personal computer at prescribed time sequences. Typically 10 to a few hundred flashes at time intervals of 3–60 s were used to take one photo. Be releasing the second flash of a series at 50% and the last one at 200% of the time interval chosen, the flash sequences were encoded, which allowed us to obtain information about the direction of flow. In the photos, the liquid crystals convected by the flow appear as strings of colored dots (see Fig. 3).

To detect the three-dimensional structures of the flow field observed, photographs were taken at different vertical and

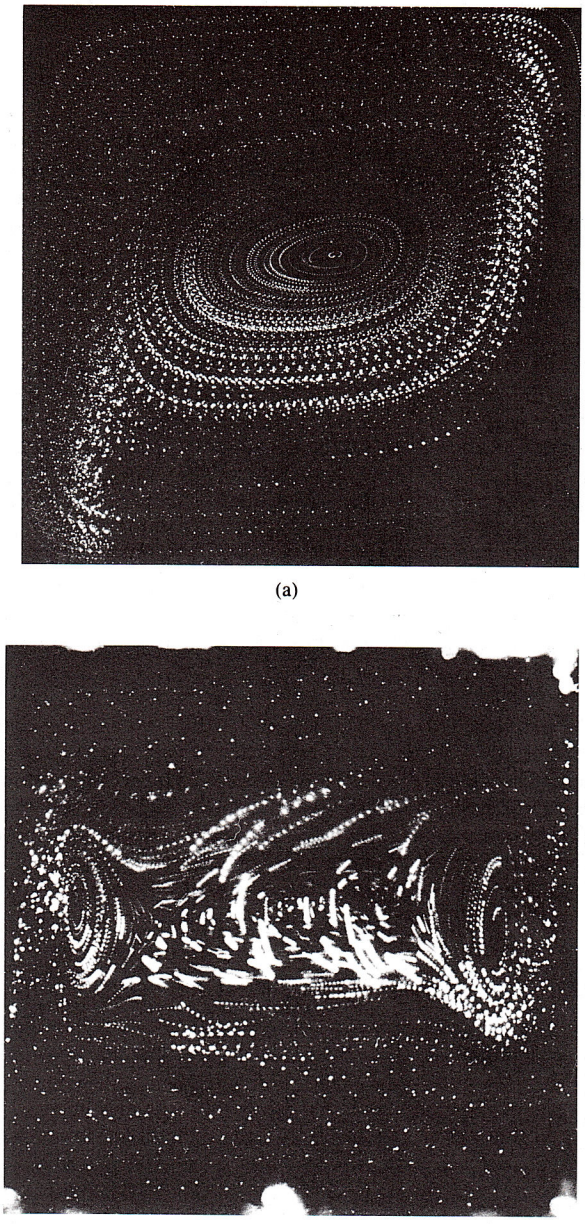

(a)

(b)

Figure 3. Photograph of convection flow visualized with the help of liquid crystals in the vertical midplane of the cavity, (*a*) Ra = 2×10^4, Pr = 6×10^3, $\Delta T = 4°C$, time interval between traces 20 s; (*b*) Ra = 2×10^6, Pr = 3×10^2, $\Delta T = 16°C$, time interval between traces 3 s.

horizontal cross sections of the cavity (from ~ 2 mm from the front wall in steps of 3 mm in the direction of the opposite wall). In this case, the width of the light sheet was 2 mm. To follow the slowly moving particles in the center of the cavity it was found very useful to use relatively thick light sheets (~ 1 cm) and long flash sequences (up to 100 flashes during several hours of exposure). This type of illumination, when applied in a horizontal plane of observation, gives long spiral paths of the particles, with the color of the particles indicating indirectly their vertical position in the cavity (see Fig. 4). Stereoscopic photos and motion pictures of the flow in the cavity have also been taken to elucidate the peculiarities of the flow.

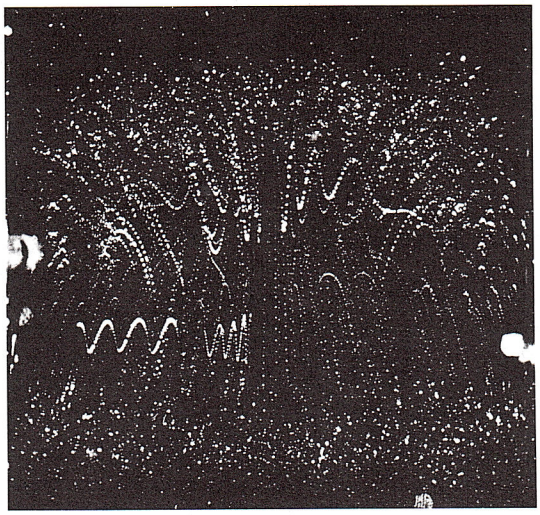

Figure 4. Photograph of convection flow in the horizontal plane $z/d = 0.55$. Ra $= 8 \times 10^4$, Pr $= 6 \times 10^3$, $\Delta T = 15°C$, time interval between traces 45 s.

EXPERIMENTAL RESULTS

General Observations

At the beginning, our interest was directed to understanding the flow in the center vertical plane of the cavity. For this purpose the observations of flow patterns and temperature fields were performed for several systems with increasing Rayleigh numbers (from 1×10^4 to 2×10^7). As an example, Fig. 5*a* shows the velocity and temperature fields at a relatively low Rayleigh number (Ra $= 2 \times 10^4$), evaluated from the photos of the cavity filled with pure glycerol. The effect of convection is already visible. Particles near the side walls follow closely the form of the cavity. In the center one vortex appears, surrounded by helical streamlines along which fluid is transported from the core to the adjacent walls. The isotherms are deformed by convection into the characteristic S shape. In the vicinity of the side walls, temperature gradients are largest and isotherms are nearly vertical. Close to the top and bottom walls, their pattern is further influenced by the thermal boundary conditions. The interior region has almost horizontal, regularly spaced isotherms. By increasing the temperature difference ΔT so that the Rayleigh number approaches 6×10^4, we observe first a horizontal elongation of the streamlines and then the formation of a secondary vortex with its center shifted toward the warmer wall. The temperature field changes very little.

Figure 5b shows the velocity and temperature field evaluated from photos for the two-vortex configuration (Ra $= 8 \times 10^4$). Further increases in the Rayleigh number were achieved by using water–glycerol mixtures as a working fluid. In this way, the viscosity of the fluid could be reduced over a wide range, thus raising the Rayleigh number but also lowering the Prandtl number of the flow. As a consequence of the Rayleigh number increase, the centers of both vortices are shifted toward the corresponding side walls (Fig. 3b). Between them, the flow becomes very complicated. However, no signs of the appearance of a third vortex could be seen, although a third vortex was predicted (for low Prandtl numbers, however) by some numerical analyses [3, 6]. The temperature field still shows very small changes compared with low Rayleigh number convection.

The dynamic development and stability of the convection were also studied in the low Rayleigh number range (10^4–10^5).

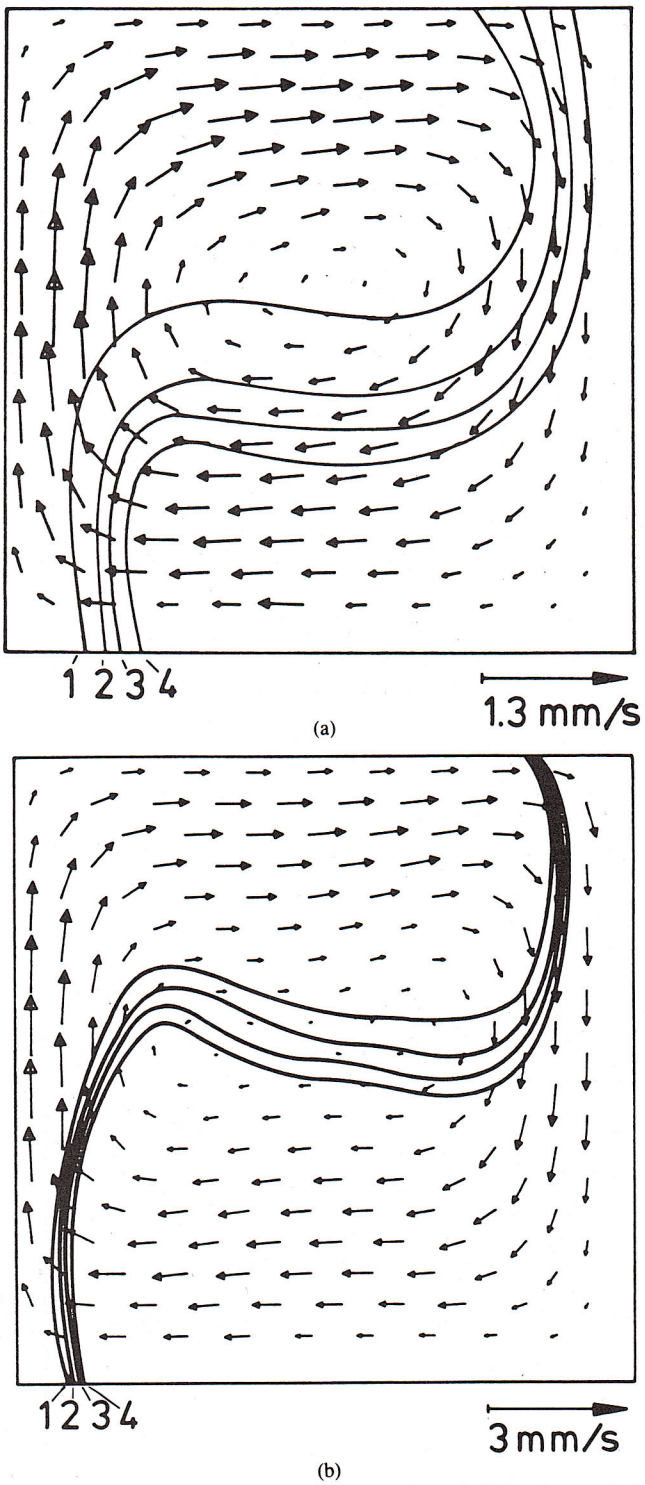

Figure 5. Velocity vectors and temperature field in the vertical midplane of the cavity, Pr $= 6 \times 10^3$, (*a*) Ra $= 2 \times 10^4$; (*b*) Ra $= 8 \times 10^4$. Isotherms refer to text.

It was found that a sudden application of a temperature gradient to the cavity walls previously in temperature equilibrium induces a strong convective flow almost immediately (within a few seconds). During the first 10 min, isotherms are first vertical and then become partly horizontal, approaching, due to convection, their S-shaped final form (Fig. 6). The flow and temperature fields assume their final structure within 20–30 min. After this time the flow seems stable. For the case of $Ra > 6 \times 10^4$, the final steady state is characterized by a double vortex in the center plane, whereas in the intermediate state a single vortex configuration is observed.

Long time tests (up to 48 h) were performed to check the stability of the flow structure. For this purpose a movie camera, working at a very low frame period (10–60 s), was used. These observations have not shown any significant short or long time fluctuations of the flow structure within the vertical center plane of the cavity.

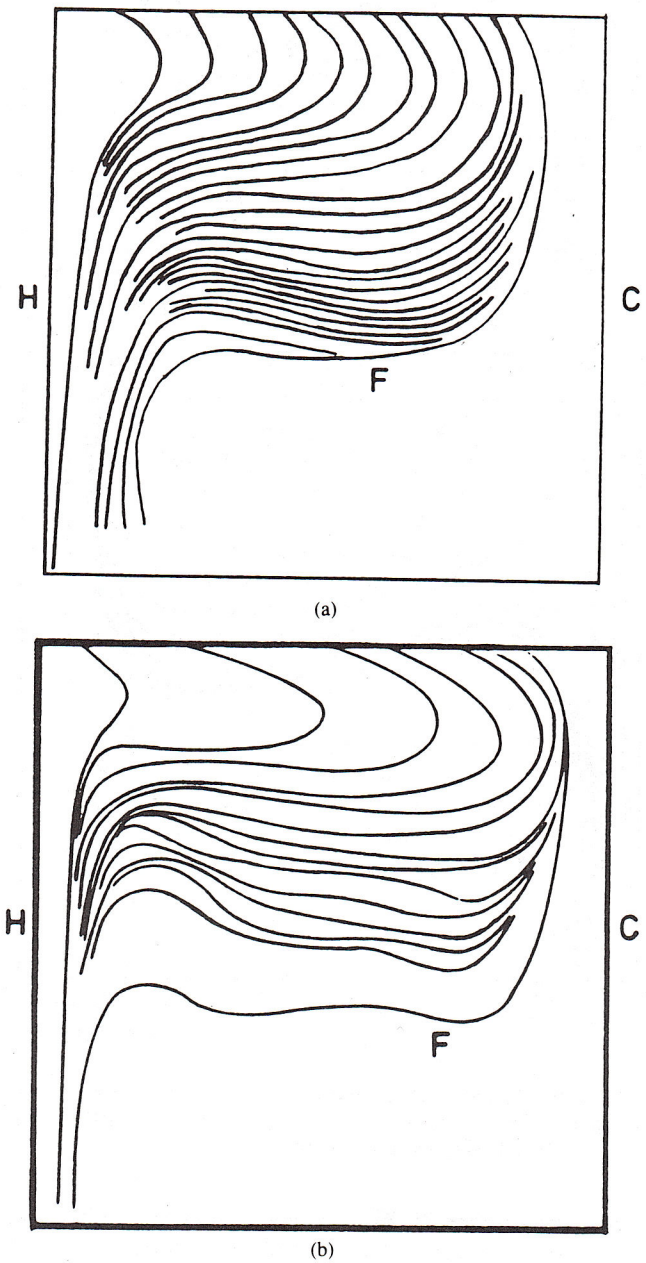

Figure 6. Development in time of the isotherm 27°C (red), Pr = 6×10^3. Time interval between isotherms 2 min. F, steady-state isotherm, (*a*) Ra = 2×10^4; (*b*) Ra = 9×10^4.

Three-Dimensional Structures

To elucidate the configuration of the flow field, systematic observations have been made for several vertical and horizontal cross sections of the cavity. To observe the transition between the one-roll and two-roll systems, the Rayleigh number was changed gradually from 10^4 to 10^5, by changing the temperature difference ΔT between the warm and cold walls (see Fig. 7). At small temperature gradients, as mentioned before, only one vortex is observed in the vertical midplane of the cavity. The center of this vortex is not in the middle of the plane but shifted toward the cold wall. At the

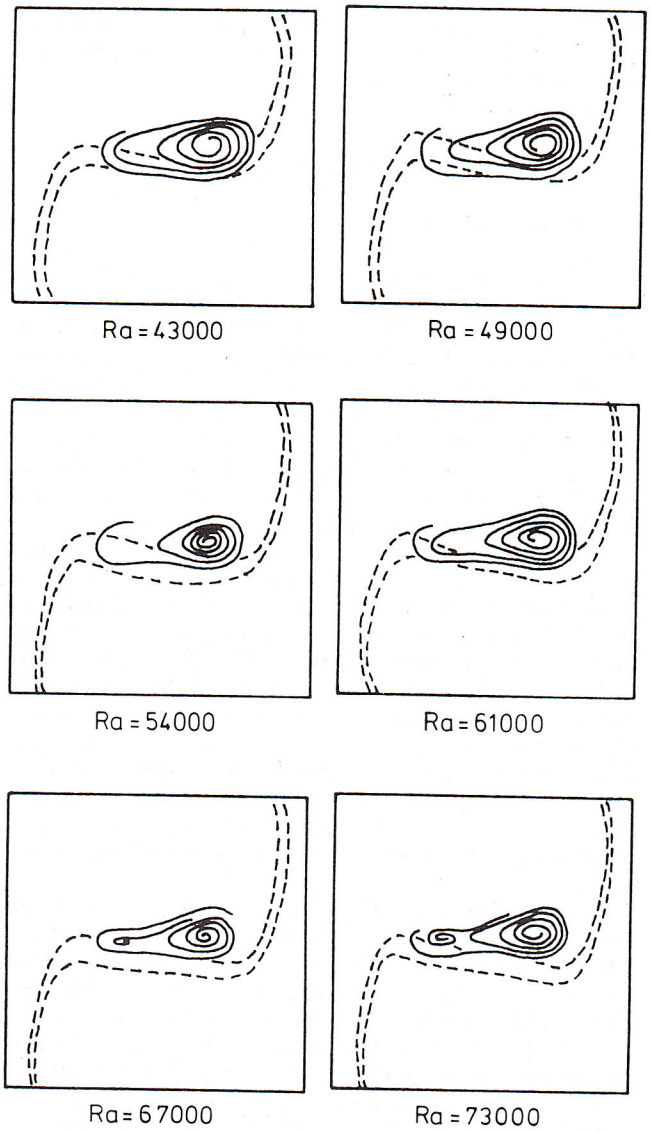

Figure 7. Transition from one-roll to two-roll convection. Pr = 6×10^3; Rayleigh number changes gradually from 4.3×10^4 to 7.3×10^4.

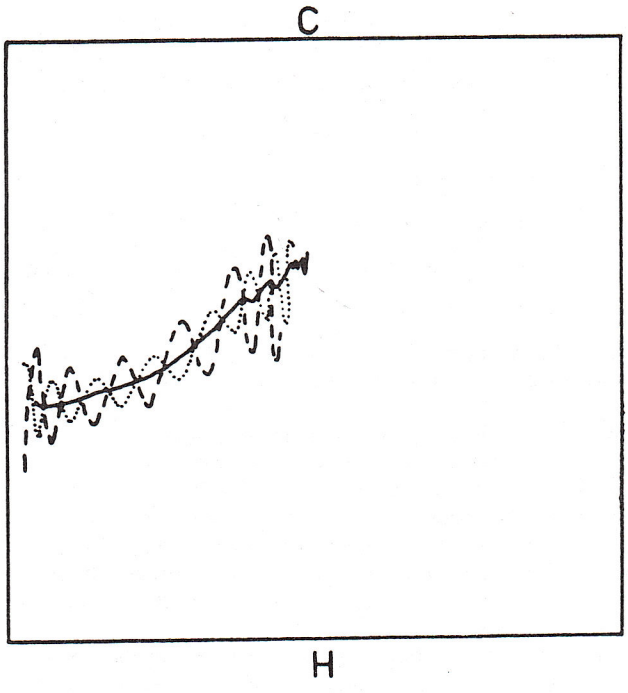

Figure 8. Streamlines in the region of the vortex core copied from the photographs. The horizontal plane $z/d = 0.55$, Pr = 6 $\times$ 10^3, (*a*) Ra = 2 $\times$ 10^4; (*b*) Ra = 8 $\times$ 10^4.

front and back walls, respectively, its ends are curved toward the hot wall (Fig. 8*a*), and hence the centerline of the vortex is concave with respect to the hot wall. In the neighborhood of the vortex center, and flow is spiraling from the back and front walls to the plane of symmetry. There the flow follows outwardly directed helical paths, and then, in the outer wall regions, it sprials to the front or back walls, respectively, and finally the motion is transformed into an inward spiral directed to the focal points on these walls. From our experiments, it was not possible to deduce whether closed streamlines exist. Approximately, the flow pattern appears like a superposition of the aforementioned concave vortex on which two counterrotating ring vortices separated by the plane of symmetry are riding.

A strict topological interpretation of the flow structure can be obtained by characterizing the field in terms of its singularities—foci, nodes, and saddlepoints—as proposed by Dallman [10]. Besides the singularities in the corners and the edges of the cubic cavity, three other singularities appear, one within the plane of symmetry, one on the front wall, and one on the back wall. These are foci with respect to the previously mentioned planes and saddlepoints in a plane orthogonal to them. In our experiment, it seems as if the two focal points on the walls are connected by a streamline with the focus on the center plane. Figure 9 displays the topological structure just discussed.

At higher Rayleigh numbers (Ra $\approx$ 6 $\times$ 10^4), a second vortex appears in the plane of symmetry that has the same sense of rotation as the first vortex. As a consequence, the former single focus in the plane of symmetry is split up into two foci that represent the centers of the spirals and a saddlepoint between them. From the centers of both vortices, the fluid spirals outwards toward the edges and side walls of the cavity (Fig. 8*b*). On the front and back walls, however, only one vortex arrives. Careful observation of the particle traces in horizontal and vertical planes shows that the vortex core next to the hot wall forms nearly a straight line, while the other vortex is bent back to the hot wall in the same manner as in the one-vortex system. About midway between the plane of symmetry and the front or back wall, respectively, one of these vortices disappears. The second vortex appears to be twisted with its ends around the first one (see Figs. 4 and 8b). In addition, the flow pattern in the outer regions remains nearly unaffected compared with the one-vortex system. A diagram of the topological structure is given in Fig. 10.

Comparing the topological structures displayed in Figs. 9

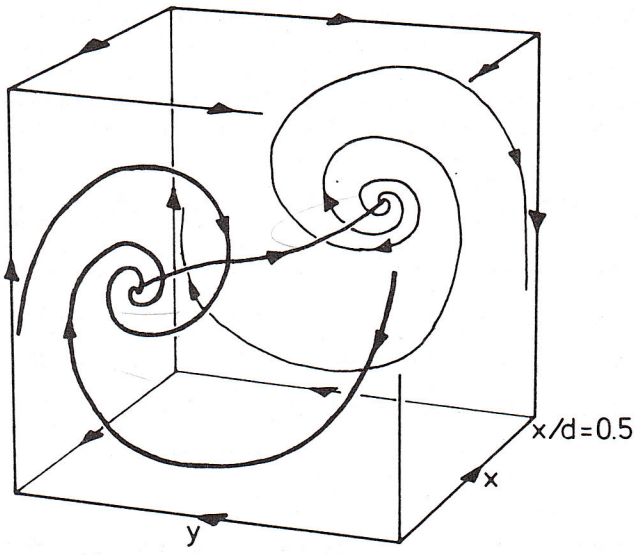

Figure 9. Principal topological structures of the one-roli system.

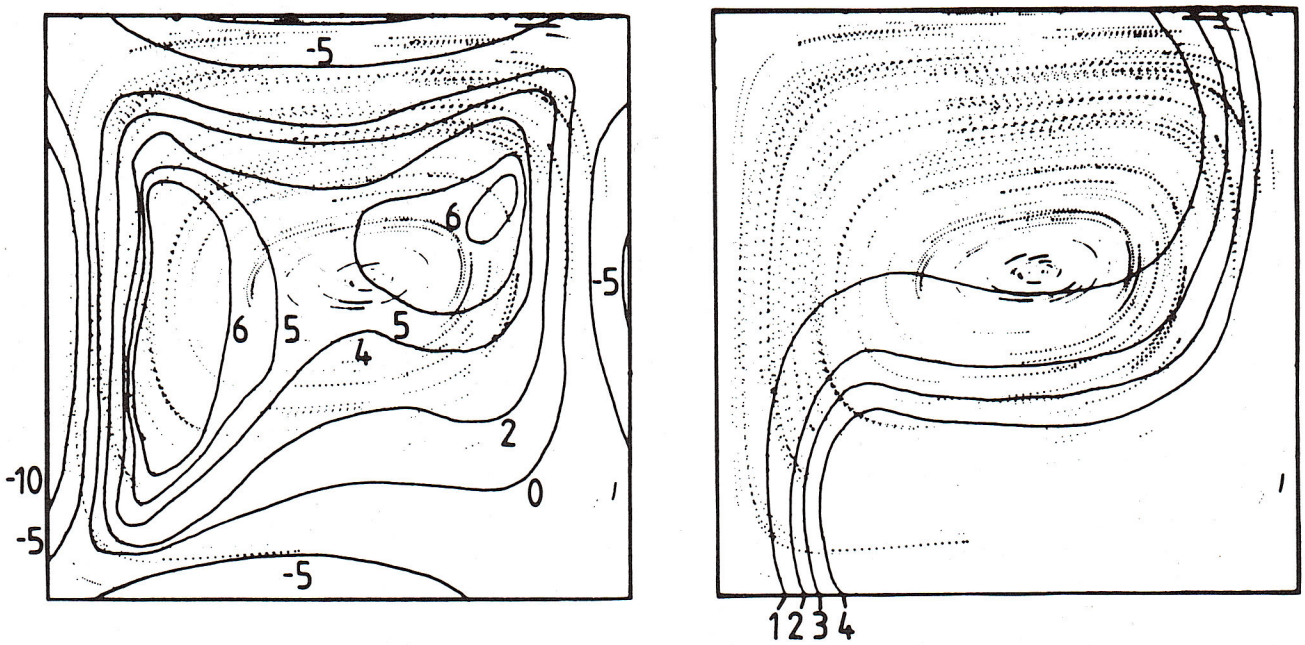

Figure 13. (*a*) Isovorticity lines and (*b*) isotherms at the vertical midplane, displayed in the photos of the streamlines; the one-roll system. Vorticity values 10^{-3} s^{-1}; for discussion of isotherms, see text. Pr = 6 × 10^3, Ra = 2 × 10^4.

front with the back wall is strongly bent, having almost a U shape. This is also true for the "cold" sprial (the one closer to the cooled wall) for the case of two-roll convection. Moreover, this vortex at approximately 25% of cavity depth disappears by twisting around the "hot" one. The "hot" vortex, however, is nearly straight.

Numerical solutions of Mallinson and de Vahl Davis indicate also that for Pr > 10 (and cavities having respect ratios greater than 1), the three-dimensional effects are confined to a thin region adjacent to the front and back walls. In our case, however (for a cavity with an aspect ratio of 1), this region seems to be much larger, covering almost one-fourth of the cavity width.

The question arises as to which of the approximations involved in numerical analysis are the main sources of the observed differences between the structures just described and the straight, symmetrical spirals predicted numerically by Mallinson and de Vahl Davis [3]. In our case, the violation of two assumptions of the numerical analysis can be involved: the Boussinesq approximation, which neglects the temperature

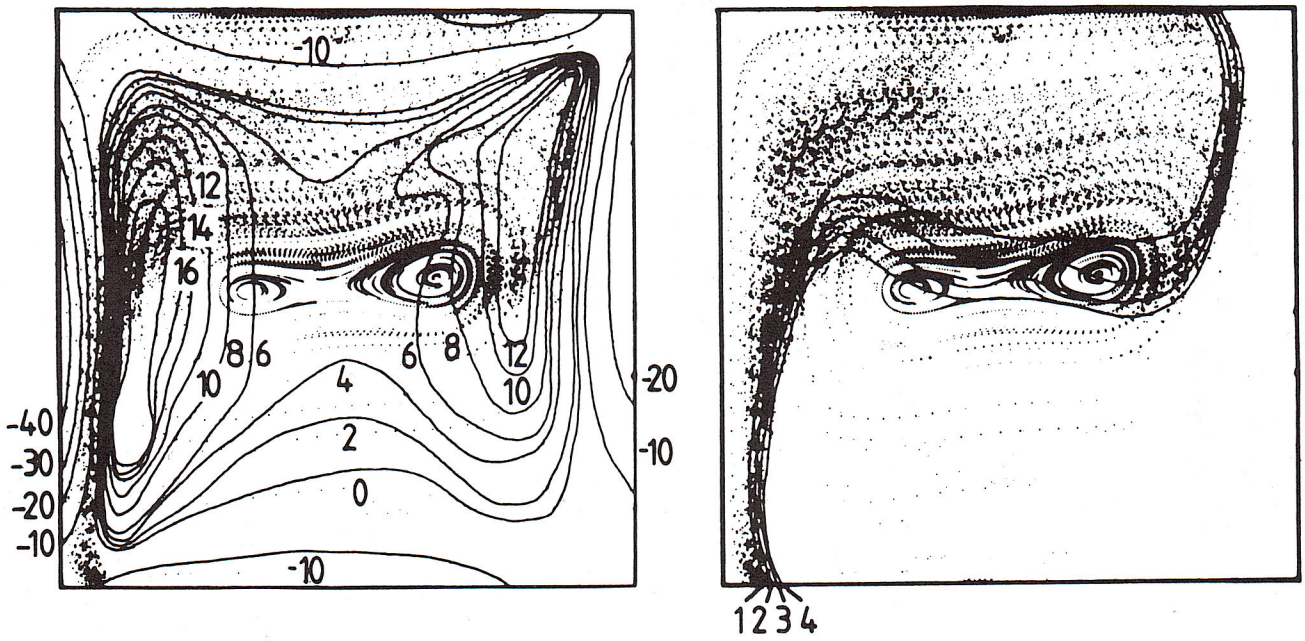

Figure 14. (*a*) Isovorticity lines and (*b*) isotherms at the vertical midplane, displayed in the photos of the streamlines; the two-roll system. Vorticity values 10^{-3} s^{-1}; for discussion of isotherms, see text. Pr = 6 × 10^3, Ra = 8 × 10^4.

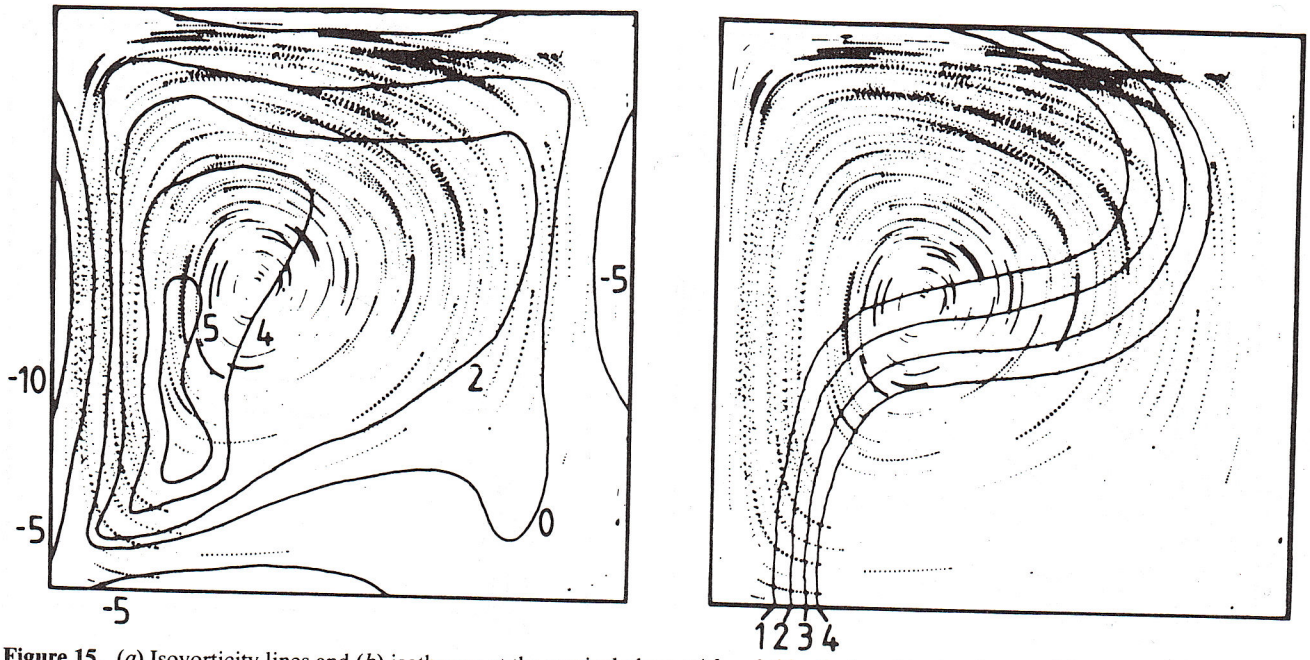

Figure 15. (*a*) Isovorticity lines and (*b*) isotherms at the vertical plane $x/d = 0.08$, displayed in the photos of the streamlines; the one-roll system. Vorticity values $\times 10^{-3}$ s^{-1}; for discussion of isotherms, see text. Pr $= 6 \times 10^3$, Ra $= 2 \times 10^4$.

dependence of viscosity, and the adiabatic approximation for the heat conductivity of the side walls. The effects of variable properties of the fluid on natural convection were the subject of several investigations [2, 13]. In the case of a liquid medium, the temperature dependence of viscosity can be important. The temperature differences present in our cavity generate local viscosity changes from 40% (for $\Delta T = 4$°C) to more than 100% (for $\Delta T = 15$°C) for the case of glycerol as a flow medium. This changes the convective flow, reducing the flow velocity locally in the colder wall regions and increasing it in the core and in the warmer parts of the cell. It surely provides an explanation for the asymmetry of the vertical velocity profile observed in the experiment (compare Figs. 11 and 12). This asymmetry of the vertical component of the convection velocity must, from the point of continuity, be compensated by additional balancing motions—toward the side walls at the cooled side of the cavity and in the direction of the center at its heated side. This lateral motion may provide an explanation of

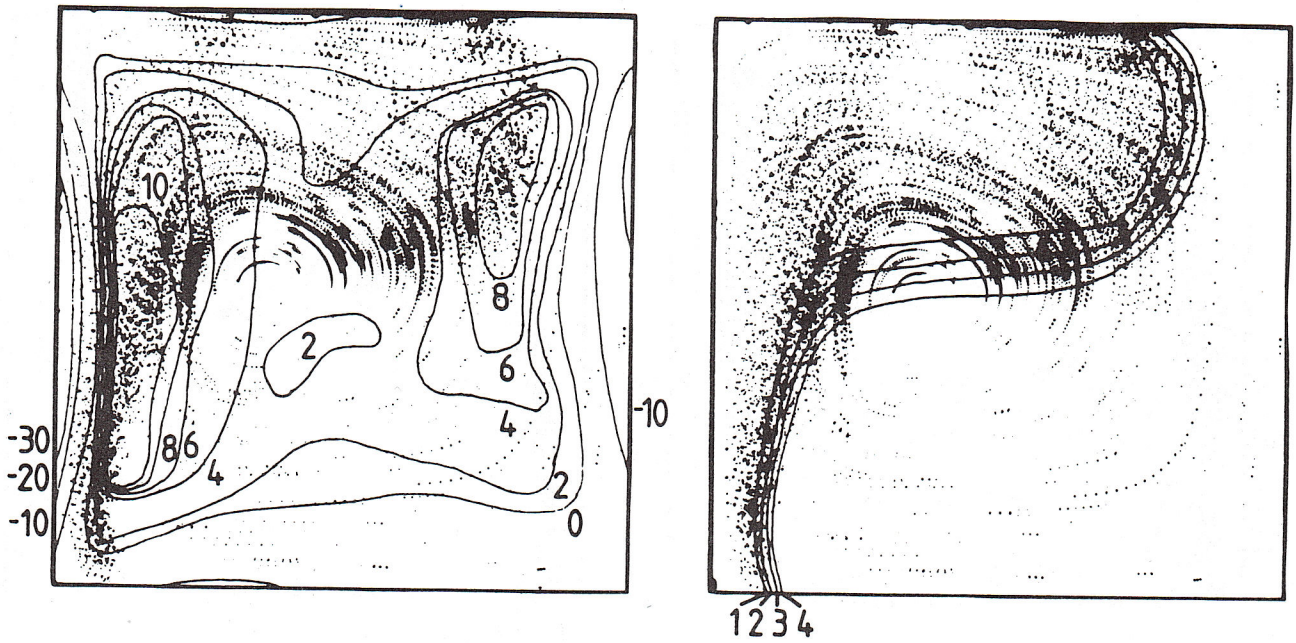

Figure 16. (*a*) Isovorticity lines and (*b*) isotherms at the vertical plane $x/d = 0.05$, displayed in the photos of the streamlines; the two-roll system. Vorticity values $\times 10^{-3}$ s^{-1}; for discussion of isotherms, see text. Pr $= 6 \times 10^3$, Ra $= 8 \times 10^4$.

the U bending observed for the vortex core. However, there are strong indications that for water as a flow medium, where the viscosity does not change so much with temperature, the vortex core also shows a considerable curvature. If global parameters of the convection are of interest, these changes seem to have negligible influence on the heat transfer rate, as the variation in the viscosity, according to MacGregor and Emery [2], is usually neglected.

The effect of thermal boundary conditions on the side walls has also been discussed in the literature and tested both numerically [14] and experimentally [15, 16]. It was concluded that thermal boundary conditions on the top and bottom walls would alter the solutions significantly only in the immediate vicinity of these boundaries and have very little influence on the flow in the central region. Mallinson [14] defined a nondimensional parameter $\tau\delta$ that indicates whether the wall insulation is sufficiently large to assume adiabatic boundaries. If τ is the ratio of the heat conductivity of the fluid to that of the wall material and δ is the ratio of the cavity width to the wall thickness, then for $\tau\delta > 10$ the difference in heat transfer between a cavity having ideal conducting side walls and a cavity with adiabatic walls is neglible. In our case, with 8 mm Perspex walls and glycerol as the working fluid, $\tau\delta \approx 15$ and the above-mentioned condition is fulfilled.

Another problem is heat exchange through the walls between the fluid inside the cavity and the external atmosphere surrounding the cavity. These heat losses can become comparable with the main heat flux for a cavity filled with gas, as shown by Morrison and Tran [15]. In the present case of a cavity filled with a fluid and relatively thick Perspex walls, the heat losses through the side walls are below 1% of overall heat transfer. Therefore, the influence of nonideal adiabatic side walls on global convection parameters (Nusselt number) is negligible in our case. However, one can expect that nonadiabatic boundaries deform strongly the flow structures in their vicinity.

As we have already mentioned, the transition from the one-roll to the two-roll configuration is determined by the balance between heat transfer due to conduction and convection. According to the two- and three-dimensional numerical simulation of Mallison and de Vahl Davis [3] this transition occurs if the Rayleigh number surpasses 6×10^4. In the three-dimensional case, close to the side walls, this condition seems not to be sufficient. The viscous boundary layer and the thermal conduction of the side walls, generally negligible for the overall heat transfer, locally deform the temperature and velocity field. It can be seen in Fig. 16*b* that the local negative temperature gradients present in the cavity midplane disappear close to the side walls, and isotherms become similar to those observed in the one-roll convection mode at low Rayleigh number (Figs. 5*a* and 13*b*). Evidently, the conditions necessary to generate the secondary roll are not fulfilled at the side walls, so the two vortex cores present in the midplane combine in the neighborhood of the wall.

CONCLUDING REMARKS

Three-dimensional steady-flow structures present in the convective flow in the cubic cavity were defined by a set of critical points and the interconnecting streamlines. The transition observed from one-roll to two-roll convection undergoes a change in the number of critical points (local topological bifurcation) [17]. Also, global topological structure changes (reversal of direction of streamlines between singularities) occur. From the experimental observations, it can be concluded that transition between these two types of flow is continuous. It would be interesting to find out how the topological structure of the flow follows this transition. Comparison of the observed flow structures with three-dimensional numerical simulations shows several severe discrepancies, which are due partly to the Boussinesq idealization of fluid properties. However, a better explanation of these discrepancies needs further numerical and experimental research of three-dimensional convective flows.

We wish to thank Dr. U. Dallmann of DFLVR Göttingen for his help and fruitful discussions concerning topological problems of the flow.

NOMENCLATURE

d	dimension of cavity, m
g	acceleration due to gravity, m/s^2
Pr	Prandtl number
Ra	Rayleigh number
T	temperature, °C
ΔT	wall temperature difference ($= T_h - T_c$), °C

Greek Symbols

α	thermal diffusivity, m^2/s
β	coefficient of cubic thermal expansion, m^3/K
δ	ratio of cavity width d to the wall thickness, dimensionless
τ	ratio of heat conductivity of the fluid to that of the wall material, dimensionless
ν	kinematic viscosity, m^2/s

Subscripts

c	cold wall
h	hot wall

REFERENCES

1. Batchelor, G. K., Heat Transfer by Free Convection Across a Closed Cavity between Vertical Boundaries at Different Temperatures, *Q. Appl. Math.*, **12**, 209-233, 1954.
2. MacGregor, R. K., and Emery, A. F., Free Convection through Vertical Plane Layers—Moderate and High Prandtl Number Fluids, *ASME J. Heat Transfer*, **91**, 391-404, 1969.
3. Mallinson, G. D., and de Vahl Davis, G., Three-Dimensional Natural Convection in a Box: A Numerical Study, *J. Fluid Mech.*, **83**, 1-31, 1977.
4. de Vahl Davis, G., Laminar Natural Convection in an Enclosed Rectangular Cavity, *Int. J. Heat Mass Transfer*, **11**, 1675-1693, 1968.
5. Phillips, T. N., Natural Convection in an Enclosed Cavity, *J. Comput. Phys.*, **54**, 365-381, 1984.
6. Markatos, N. C., and Pericleous, K. A., Laminar and Turbulent Natural Convection in an Enclosed Cavity, *Int. J. Heat Mass Transfer*, **27**, 755-772, 1984.
7. Elder, J. W., Laminar Free Convection in a Vertical Slot, *J. Fluid Mech.*, **23**, 77-98, 1965.
8. Yin, S. H., Wung, T. Y., and Chen, K., Natural Convection in Air Layer Enclosed within Rectangular Cavities, *Int. J. Heat Mass Transfer*, **21**, 307-315, 1978.
9. Hiller, W. J., and Kowalewski, T. A., Simultaneous Measurement of Temperature and Velocity Fields in Thermal Convective Flows, in

Flow Visualization, vol. 4, Claude Veret, Ed., pp. 617–622, Hemisphere, New York, 1987.

10. Dallmann, U., Structural Stability of Three-Dimensional Vortex Flows, in *Lecture Notes in Engineering*, Proc. DFVLR International Colloquium, Bonn, March 26, 1984, Vol. 13, H. L. Jordan, H. Oertel, and K. Robert, Eds., Springer-Verlag, New York, 1985.
11. Koch, S., Experimente zur Thermokonvektion in einer kubischen Zelle, Diplomarbeit, Universität Göttingen, 1987.
12. Lugt, H. J., and Haussling, H. J., Development of Flow Circulation in a Rotating Tank, *Acta Mech.*, **18**, 255, 1973.
13. Zhong, Z. Y., Yang, K. T., and Lloyd, J. R., Variable Property Effets in Laminar Natural Convection in a Square Enclosure, *ASME J. Heat Transfer*, **107**, 133–138, 1985.
14. Mallinson, G. D., The Effect of Side-Wall Conduction on Natural Convection in a Slot, *ASME J. Heat Transfer*, **109**, 419–426, 1987.
15. Morrison, G. L., and Tran, V. Q., Laminar Flow Structure in Vertical Free Convection Cavities, *Int. J. Heat Mass Transfer*, **21**, 201–213, 1978.
16. Kim, D. M., and Viskanta, R., Effect of Wall Heat Conduction on Natural Convection Heat Transfer in a Square Enclosure, *ASME J. Heat Transfer*, **107**, 139–146, 1985.
17. Dallmann, U., Three-Dimensional Vortex Structures and Vorticity Topology, *Fluid Dyn. Res.*, **3**, 183–189, 1988.

Revised August 15, 1988